Dalton Transactions

Accepted Manuscript

This article can be cited before page numbers have been issued, to do this please use: C. Wang, L. Lystrom, H. Yin, M. Hetu, S. Kilina, S. A. McFarland and W. Sun, *Dalton Trans.*, 2016, DOI: 10.1039/C6DT02416E.

This is an *Accepted Manuscript*, which has been through the Royal Society of Chemistry peer review process and has been accepted for publication.

Accepted Manuscripts are published online shortly after acceptance, before technical editing, formatting and proof reading. Using this free service, authors can make their results available to the community, in citable form, before we publish the edited article. We will replace this *Accepted Manuscript* with the edited and formatted *Advance Article* as soon as it is available.

You can find more information about *Accepted Manuscripts* in the Information for Authors.

Please note that technical editing may introduce minor changes to the text and/or graphics, which may alter content. The journal's standard Terms & Conditions and the Ethical guidelines still apply. In no event shall the Royal Society of Chemistry be held responsible for any errors or omissions in this *Accepted Manuscript* or any consequences arising from the use of any information it contains.

ROYAL SOCIETY OF CHEMISTRY

www.rsc.org/dalton

View Article Online
DOI: 10.1039/C6DT02416E

Table of Contents Entry

Tuning the photophysics of cationic Ir(III) complexes via π-expansive ligands dramatically impacts their applications as broadband reverse saturable absorbers and in photodynamic therapy and theranostic.

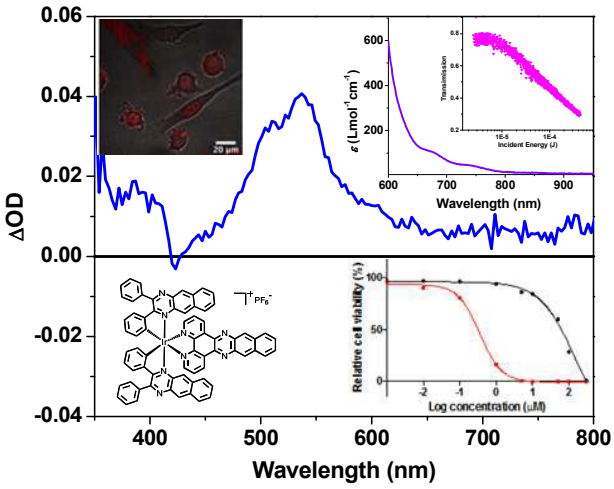

View Article Online
DOI: 10.1039/C6DT02416E

Dalton Transactions

ARTICLE

Received 00th January 20xx,
Accepted 00th January 20xx

DOI: 10.1039/x0xx00000x

www.rsc.org/

Increasing the triplet lifetime and extending the ground-state absorption of cationic biscyclometalated Ir(III) complexes by tuning ligand π-conjugation for applications in reverse saturable absorption and photodynamic therapy

Chengzhe Wang,[a] Levi Lystrom,[a] Huimin Yin,[b] Marc Hetu,[b] Svetlana Kilina,[a] Sherri A. McFarland*[b] and Wenfang Sun*[a]

The synthesis, photophysics, reverse saturable absorption, and photodynamic therapeutic effect of six cationic biscyclometalated Ir(III) complexes (**1-6**) with extended π-conjugation on the diimine ligand and/or the cyclometalating ligands are reported in this paper. All complexes possess ligand-localized $^1\pi,\pi^*$ absorption bands below 400 nm and charge-transfer absorption bands above 400 nm. They are all emissive in the 500-800 nm range in deoxygenated solutions at room temperature. All complexes exhibit strong and broad triplet excited-state absorption at 430-800 nm, and thus strong reverse saturable absorption for ns laser pulses at 532 nm. Complexes **1-4** are strong reverse saturable absorbers at 532 nm, while complex **6** could be a good candidate as broadband reverse saturable absorber at 500-850 nm. The degree of π-conjugation of the diimine ligand mainly influences the $^1\pi,\pi^*$ transitions in their UV-vis absorption spectra, while the degree of π-conjugation of the cyclometalating ligand primarily affects the natures and energies of the lowest singlet and emitting triplet excited states. However, the lowest-energy triplet excited states for complexes **3-6** that contain the same benzo[i]dipyrido[3,2-a:2',3'-c]phenazine (dppn) diimine ligand but different cyclometalating ligands remain the same as the dppn ligand-localized $^3\pi,\pi^*$ state, which gives rise to the long-lived, strong excited-state absorption in the visible to the near-IR region. All of the complexes exhibit a photodynamic therapeutic effect upon visible or red light activation, with complex **6** possessing the largest phototherapeutic index reported to date (>400). Interactions with biological targets such as DNA suggest that a novel mechanism of action may be at play for the photosensitizing effect. These Ir(III) complexes also produce strong intracellular luminescence that highlights their potential as theranostic agents.

Introduction

Biscyclometalated iridium (III) complexes bearing diimine ligands have attracted much interest over the past two decades because the spin-orbit coupling coefficient of iridium is among the largest, which results in very efficient intersystem crossing (ISC) in such systems.[1] This heavy-atom induced singlet-triplet mixing produces intense phosphorescence at room temperature,[2] which has been widely exploited for organic light-emitting diodes (OLEDs),[3] light-emitting electrochemical cells (LEECs),[4] biosensors,[5] and chemosensors.[6] Despite these (and other) favorable optical properties, such complexes are rarely explored in context of reverse saturable absorption (RSA),[7] probably due in part to a lack of well-established structure-property correlations with respect to organometallic complexes and RSA.

RSA is a nonlinear optic (NLO) process whereby a molecule absorbs more photons in its excited state than its ground state.[8] This NLO property can be used for optical rectification,[9] laser pulse compression and stabilization,[10] and optical switching.[11] The effectiveness of RSA is mainly governed by the ratio of absorption cross sections between the ground and excited states.[12] To produce efficient RSA with nanosecond laser pulses, a long-lived triplet excited state with strong absorption is required.[13] Transition-metal complexes (Pt,[14] Fe,[15] Ru,[16] Hg,[14i,17] Au,[14i,17] etc.) are attractive for this purpose because the heavy-atom induced SOC increases the quantum yield for triplet state formation. However, efficiently populating the triplet excited state via one-photon absorption of visible to near-IR (NIR) light (400 – 900 nm) while maintaining a large triplet state absorption cross-section and long lifetime remains a challenge.

[a] Department of Chemistry and Biochemistry, North Dakota State University, Fargo, ND 58108-6050, USA. E-mail: Wenfang.Sun@ndsu.edu
[b] Department of Chemistry, Acadia University, 6 University Avenue, Wolfville, NS B4P 2R6, Canada. E-mail: sherri.mcfarland@acadiau.ca

Electronic Supplementary Information (ESI) available: Experimental details, NTOs for the high energy and intermediate energy absorption bands, comparison of experimental and computational UV-vis absorption spectra of **1-6**, excitation spectra of **1-6**, solvent-dependent UV-vis and emission spectra and emission characteristics of **1-6**, time-resolved ns transient absorption spectra of ligands and complexes **1-6**, in vitro dose-response curves for **1-3**, confocal luminescence images of SK-MEL-28 cells dosed with **1-3** in the dark or activated by visible light, DNA photocleavage with **1-3** and visible light, See DOI: 10.1039/x0xx00000x

View Article Online
DOI: 10.1039/C6DT02416E

A long-lived triplet excited state, high triplet quantum yield, and a broad ground-state absorption in the NIR region are also desirable features for biomedical applications such as photodynamic therapy (PDT).[18] Briefly, PDT is a selective means of destroying tumors and tumor vasculature by applying a light trigger to activate an otherwise nontoxic compound called a photosensitizer (PS). The excited triplet state of the PS then reacts with ground state oxygen to produce cytotoxic reactive oxygen species (ROS) through Type I (electron transfer) or Type II (energy transfer) mechanisms. Singlet oxygen that is generated via Type II mechanism has been implicated as the most important mediator of PDT's anticancer effects.[19] Despite much promise, PDT is underutilized and is not a mainstream approach for treating cancer, owing in part to the absence of PSs with the aforementioned properties.

It has been reported that strong SOC makes direct absorption from the singlet ground state to the lowest triplet excited state possible in some Ir(III) complexes.[20] Such transitions give rise to very weak but broad ground-state absorption of visible and NIR light. For example, Ir(III) complexes bearing 2,3-diphenylbenzo[g]quinoxaline (dpbq) cyclometalating ligands[20d] possess a weak but broad ground-state absorption from 600-800 nm due to this direct absorption from the singlet ground state to the triplet excited state. This weak ground-state absorption provides another path for populating the triplet excited state in addition to ISC from the singlet excited state. On the other hand, this efficient ISC also facilities the decay of the lowest triplet excited state, reducing the triplet lifetime. Balancing these two effects is critical for developing long-lived and broadband-absorbing (in both the ground state and excited state) transition-metal complexes for RSA and PDT applications.

It is well known that the triplet excited state lifetime is mainly governed by the nature and energy of the lowest triplet excited state (T_1), which could be of metal-to-ligand charge transfer (MLCT), metal-centered (MC), ligand-to-metal charge transfer (LMCT), ligand-to-ligand charge transfer (LLCT), intraligand charge transfer (ILCT), intraligand (IL or π,π^*), or metal-to-metal charge transfer (MMCT) character, or mixtures of such states. Previous studies involving Ru(II) complexes have shown that increasing the degree of π-conjugation of certain diimine ligands can lengthen triplet lifetimes dramatically. For example, the 750-ns triplet lifetime of $[Ru(bpy)_2dppz]^{2+}$ (bpy=2,2'-bipyridine and dppz = dipyrido[3,2-a:2',3'-c]phenazine) is lengthened to 33±5 μs with the extension of the π-system by one fused benzene ring to yield $[Ru(bpy)_2dppn]^{2+}$ (dppn = benzo[i]dipyrido[3,2-a:2',3'-c]phenazine).[21] This is made possible when the lowest energy ^{3}IL state drops below ~2.1 eV, the energy of the lowest ^{3}MLCT state in typical Ru(II) polypyridyl complexes. Similarly, our own investigations with Ru(II) complexes bearing the 5-(pyren-1′-ylethynyl)-1,10-phenanthroline (5-PEP) ligand have yielded T_1 lifetimes as long as 240 μs for complexes of the type $[Ru(bpy)_2(5\text{-PEP})]^{2+}$ and 270 μs for the homoleptic $[Ru(5\text{-PEP})_3]^{2+}$.[22] In the same study, we highlighted the utility of such long-lived ^{3}IL states for PDT by demonstrating that these complexes yield the highest light potencies and largest phototherapeutic margins to date.

We have also previously demonstrated that the triplet state lifetimes of Ir(III) complexes containing π-conjugated aromatic substituents appended to diimine ligands are drastically lengthened (τ = 11.3 μs) in comparison to the analogous complexes without these substituents.[23] As observed for the π-expansive Ru(II) complexes, the long lifetimes were achieved by extending the π-conjugation of certain coordinating ligands to lower the energy of the ^{3}IL state below that of the ^{3}MLCT. Because the Ru(II) complexes bearing these highly π-conjugated ligands exhibit long-wavelength activation (>600 nm) and high singlet oxygen quantum yields,[24,25] which are attractive features for PDT, we were inspired to explore Ir(III) complexes with similar properties as PSs for PDT.

We designed six Ir(III) cyclometalated complexes (Chart 1) to interrogate the effects of extending the π-conjugation of the diimine ligand (**1-3)** versus the cyclometalating ligand (**4-6**) on the ground and triplet excited state absorption and the triplet lifetime. Their applications as reverse saturable absorbers and PSs for PDT are reported herein.

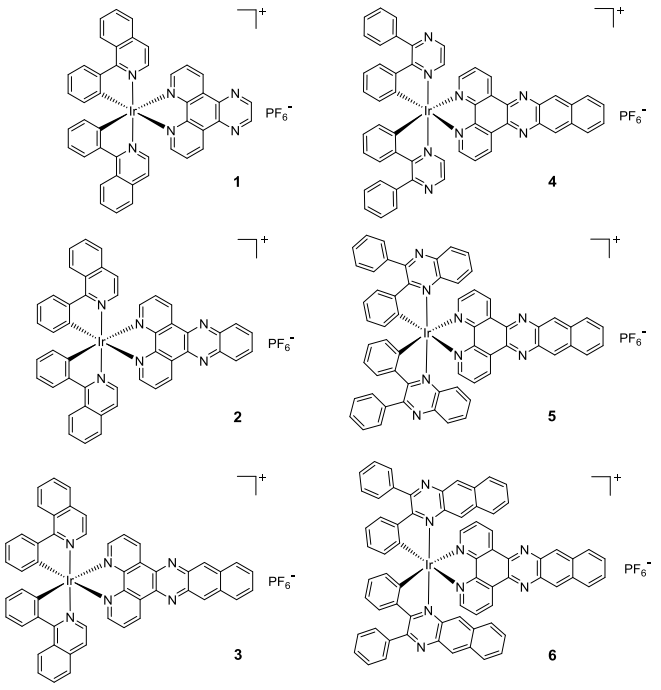

Chart 1 Structures of Ir(III) complexes **1-6**.

Results and discussion

Synthesis and characterization

The synthetic route for complexes **1–6** is shown in Scheme 1, and the synthetic details and characterization data are provided in the Experimental Section. All of the ligands were synthesized according to the literature procedures.[20d,26] The procedure reported by Nonoyama was followed to convert the cyclometalating ligands into the chloro-bridged dinuclear Ir(III) precursors.[27] Reactions of the dinuclear Ir(III) complexes with the corresponding diimine ligand in

View Article Online DOI: 10.1039/C6DT02416F

the presence of $AgSO_3CF_3$ catalyst in mixed CH_2Cl_2/CH_3OH solvent[28] gave the desired mononuclear Ir(III) complexes **1-6**. The intermediate compounds were confirmed by ^1H NMR spectroscopy, while the ligands and the Ir(III) complexes were characterized by ^1H NMR, HRMS, and elemental analyses.

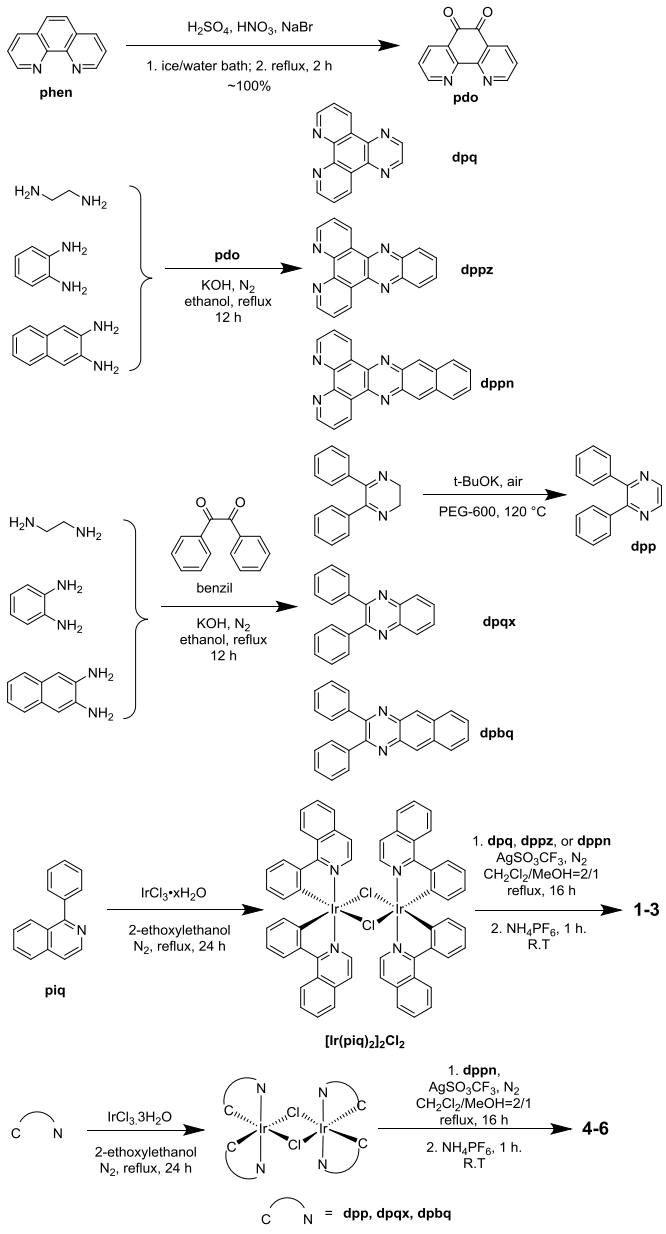

Scheme 1 Synthetic routes for complexes **1-6**.

UV-vis absorption

The UV-vis absorption of all of the ligands and complexes were measured in acetonitrile solutions. Concentration dependence experiments (2×10^{-6} mol/L to 1×10^{-4} mol/L solutions) indicated that Beer's law was obeyed, suggesting the absence of ground state aggregation due to the octahedral geometry of the Ir(III) complexes.

All complexes showed intense and structured UV-vis absorption at wavelengths below 350 nm (below 320 nm for complexes **1-3**) (Figure 1). The magnitudes of their molar extinction coefficients in this region (~ 5 – 10 × 10^4 L/mol.cm, Table 1) are consistent with $^1\pi,\pi^*$ transitions (referred to as IL when incorporated into a metal complex) localized on the diimine or the cyclometalating ligands. This assignment was supported by the natural transition orbitals[29] (NTOs, ESI Table S1) obtained from the TDDFT calculations, which also indicated minor contributions from charge transfer (CT) transitions in this energy range. Figure 1A clearly shows that the most intense band observed for complexes **1-3** in this region shifted bathochromically in a systematic manner with increasing π-conjugation of the diimine ligand. In contrast, there was no shift in the most intense UV band (~320 nm) for **4-6**, but the molar extinction coefficients were noticeably different. The NTOs (ESI Table S1) revealed considerable contributions from the CT transitions (*i.e.* ^{1}MLCT, ^{1}LLCT, and ^{1}ILCT) in addition to the major dppn-localized $^1\pi,\pi^*$ transition for **5** and **6**, which do not contribute as much for **4** due to the smaller π-conjugation of the cyclometalating ligand in **4**. The larger contributions from the CT transitions decreased the intensity of these high-energy absorption bands for **5** and **6** relative to that observed for **4**.

Table 1 Photophysical data of complexes **1-6** in acetonitrile.

	λ_{abs} / nm (ε / 10^4 L.mol^{-1}.cm^{-1})	λ_{em} / nm (τ_{em} / μs; Φ_{em})	$\lambda_{T1\text{-}Tn}$ / nm (τ_T / μs; $\varepsilon_{T1\text{-}Tn}$ / 10^4 L.mol^{-1}.cm^{-1}; Φ_T)
1	257 (7.19); 289 (5.65); 340 (2.01); 378 (1.36); 434 (0.7)	588 (2.98; 0.22)	516 (3.19; 7.6; 0.25)
2	278 (6.86); 354 (2.16); 379 (1.61); 434 (0.58)	590 (0.40; 0.034)	518 (0.43; 19.2; 0.052)
3	291 (6.84), 322 (9.21), 395 (1.68), 420 (1.79)	591 (2.69; 0.026)	536 (35.7; 19.9; 0.12)
4	322 (9.93), 397 (1.66), 418 (1.87), 456 (0.65)	554 (2.52; 0.015)	537 (36.9; 11.1; 0.23)
5	319 (8.21), 375 (3.49), 394 (3.19), 417 (2.12), 464 (0.87)	629 (2.39; 0.083)	537 (39.6; 19.6; 0.069)
6	322 (9.29), 399 (2.51), 417 (2.57), 476 (0.92), 537 (0.39)	553 (0.06; -[a]), 774 (-;-)[a]	537 (15.1; 31.8; 0.054)

[a] Too weak to be measured.

The less intense bands in the range of 320-400 nm for complexes **1-3** and 350-450 nm for **4-6** have mixed $^1\pi,\pi^*/^1$LLCT/^{1}MLCT/^{1}ILCT/^{1}LMCT character in view of their relatively large extinction coefficients (which are on the order of 2 – 4 × 10^4 L/mol.cm) and the NTOs shown in ESI Table S2. When the π-conjugation was increased on the diimine ligands, the intensities of these absorption bands gradually increased from complex **1** to complex **3**. In line with this trend, the increased π-conjugation on the cyclometalating ligands also led to increased absorption for the band near 420 nm for complexes **4-6**. However, the intensity of the band at ca. 400 nm for complexes **4-6** does not follow this trend, with complex **5** possessing the strongest absorption and complex **4** showing the weakest absorption among these three complexes. This can be explained by the different characters of contributing transitions to this band (see the NTOs for S_{10} of complex **4**, S_9, S_{10}, and S_{18} of complex **5**, and S_{15}, S_{16}, and S_{20} of complex **6** in Table S2). As these NTOs indicate, the major contributing transitions to this band in complex **4** are $^1\pi,\pi^*$(dppn)/^{1}MLCT; while in complex **5** are the $^1\pi,\pi^*$(dppn)/^{1}MLCT mixed with ^{1}ILCT/^{1}LLCT. The additional contribution from the ^{1}ILCT/^{1}LLCT transitions in

complex **5** makes this band stronger than that in complex **4**. On the contrary, the charge transfer transitions (*i.e.* ^{1}LLCT/^{1}MLCT/^{1}ILCT) contribute predominantly to this band in complex **6**, with minor contribution from the $^1\pi,\pi^*$(dpbq). The predominant charge transfer nature of this band in complex **6** accounts for the decreased intensity of this band in comparison to the predominant $^1\pi,\pi^*$(dppn)/ MLCT band in complex **5** in the similar energy region.

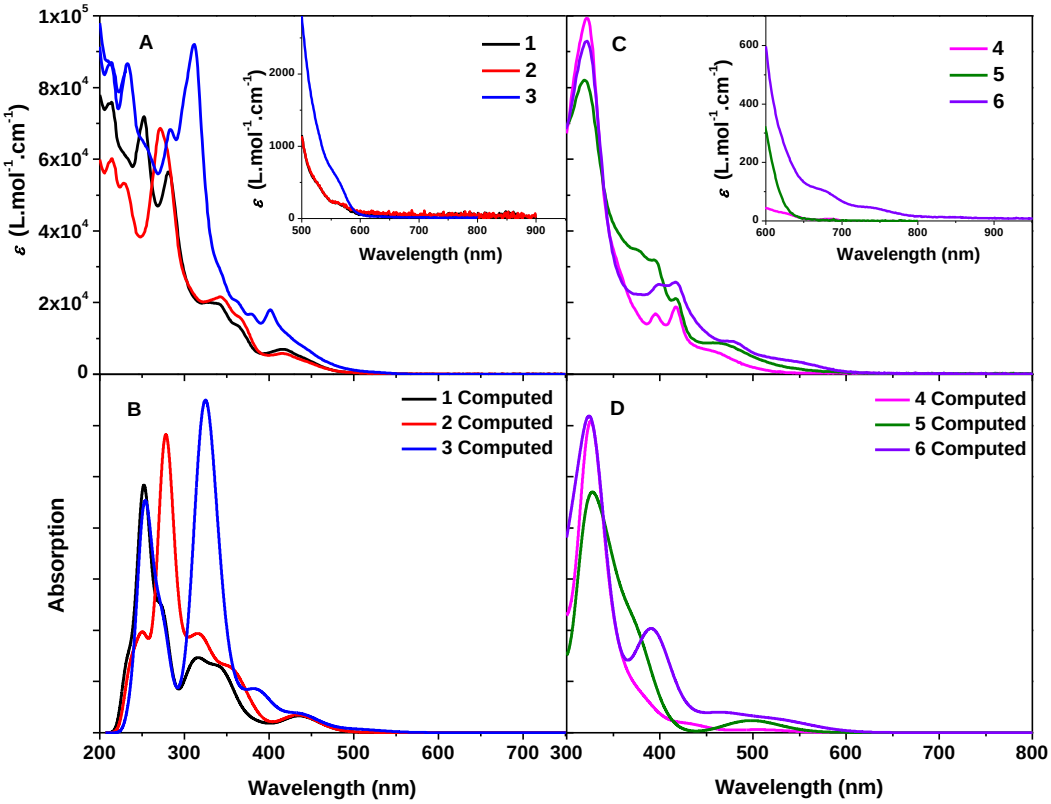

Fig. 1 UV-Vis absorption spectra of complexes **1-6** in acetonitrile. Panels A and C: experimental spectra; Panels B and D: calculated spectra.

In addition to the aforementioned structured absorption bands, each complex exhibited broad and featureless absorption band(s) at 400-500 nm for complexes **1-3** and 450-600 nm for complexes **4-6**. Considering the moderate intensity ($\varepsilon \sim 10^3 - 10^4$ L/mol.cm) and the structureless features, we attribute these bands mainly to charge-transfer transitions (^{1}MLCT/^{1}LLCT and/or ^{1}ILCT), likely mixed with some $^1\pi,\pi^*$ character. This assignment was supported by the TDDFT calculations (see NTOs illustrated in Table 2 for these low-energy absorption bands). For the lowest-energy transitions in these complexes (S_1 state), the promoted electrons are all exclusively localized on the diimine ligand except for complex **6**, in which the electron is delocalized on the cyclometalating dpbq ligand and the *d*-orbital of the Ir(III). While the holes are primarily on the phenyl rings of the cyclometalating ligand and the *d*-orbital of the Ir(III) except for complex **4**, which has the hole localized on part of the dppn ligand. According to the electron and hole distributions, the nature of the S_1 states for complexes **1-3** and **5** can be attributed to ^{1}MLCT/^{1}LLCT; while for complex **4** it has $^1\pi,\pi^*$/^{1}ILCT character, and complex **6** has major ^{1}ILCT/^{1}MLCT character mixed with some contributions from $^1\pi,\pi^*$/^{1}LMCT.

When the π-conjugation on the diimine ligand was increased on going from complex **1** to complex **3**, the energy of the diimine ligand localized π^* orbital decreased (*i.e.* the LUMO energy decreased, see the calculated ground-state energy diagram displayed in Fig. 2), while the π(Ph)/*d*(Ir) based HOMO energy was unchanged, resulting in a decreased HOMO-LUMO gap. This systematic decrease in the energy of S_1 from **1** to **3** is evident as a red-shift in the lowest-energy absorption bands. Although the nature of S_1 differed between **4-6**, there was also a systematic gradual decrease in the S_1 state with increased π-conjugation on the cyclometalating ligands.

A close examination of the UV-vis absorption spectra of these complexes revealed a very weak tail beyond 500 nm for complexes **1-3** and past 600 nm for complexes **4-6**. As reported for other Ir(III) complexes,[20] these bands are most likely due to direct S_0-T_n absorption via the spin-forbidden $^3\pi,\pi^*/^3$CT transition. Extending the π-conjugation on the cyclometalating ligand dramatically expanded this band into the red to near-IR region, especially for complex **6** , which could potentially be exploited for both RSA and PDT, as discussed in the introduction.

View Article Online
DOI: 10.1039/C6DT02416E

Table 2 Natural transition orbitals (NTOs) representing transitions contributing to the low-energy absorption bands of complexes **1–6** in CH_3CN.

	S_n	Holes	Electrons		S_n	Holes	Electrons
1	S_1 464 nm f = 0.006		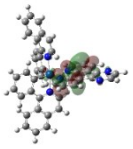	**4**	S_1 507 nm f = 0.021	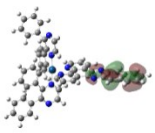	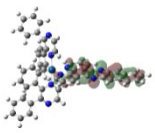
	S_2 436 nm f = 0.112	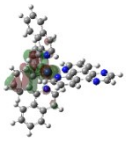	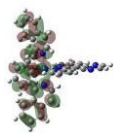		S_3 437 nm f = 0.008	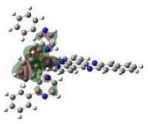	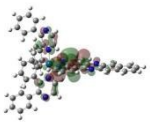
2	S_1 490 nm f = 0.002		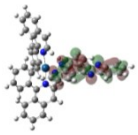	**5**	S_1 512 nm f = 0.011	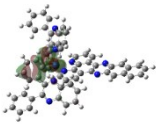	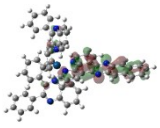
	S_2 449 nm f = 0.009	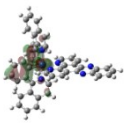	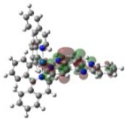		S_2 506 nm f = 0.019	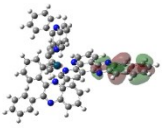	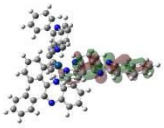
	S_3 435 nm f = 0.107	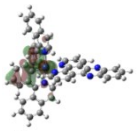	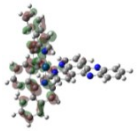		S_3 494 nm f = 0.055	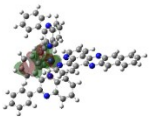	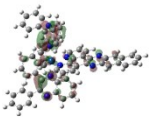
3	S_1 533 nm f = 0.001	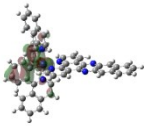	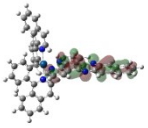	**6**	S_1 541 nm f = 0.050	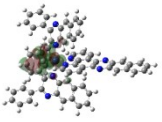	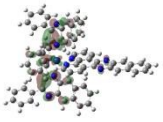
	S_2 504 nm f = 0.021	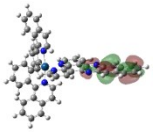	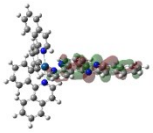		S_2 510 nm f = 0.016	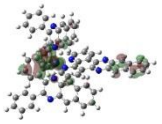	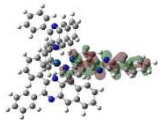
	S_5 435 nm f = 0.109	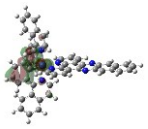	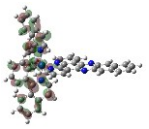		S_6 470 nm f = 0.049	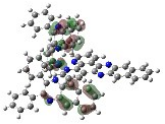	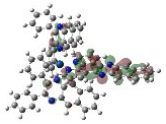

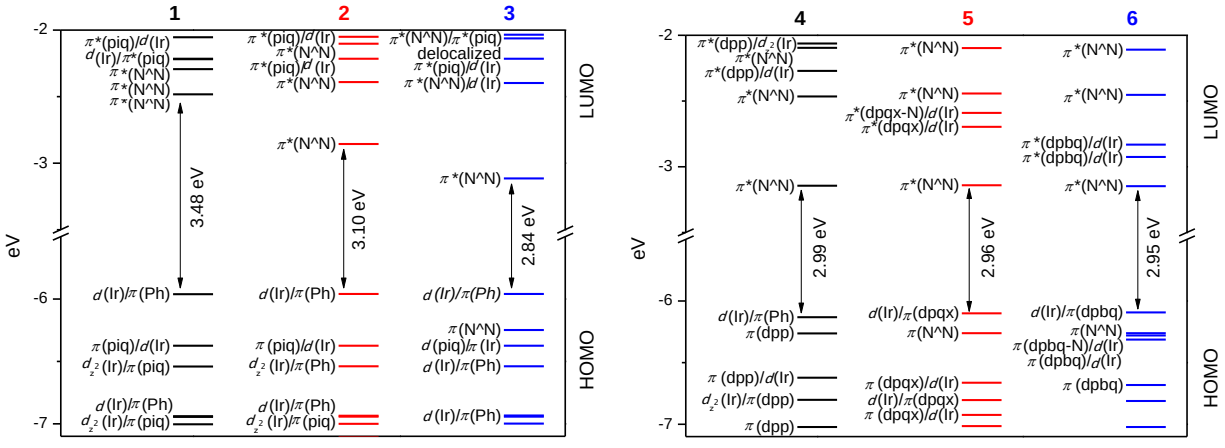

Fig. 2 Ground-state energy diagram for complexes **1-6** in CH_3CN.

View Article Online
DOI: 10.1039/C6DT02416E

Dalton Transactions

ARTICLE

Photoluminescence

The room temperature emission from complexes **1-6** in different solvents was studied. The observed luminescence was sensitive to oxygen, with lifetimes in the range of hundreds of nanoseconds to several μs in deoxygenated solutions (except for complex **6**, *vide infra*). The magnitude of measured Stokes shifts (the difference between the emission energy and the excitation energy) were in the range of 5015-6946 cm^{-1}. These facts suggested that the observed emission in all cases was phosphorescence.

Fig. 3 illustrates the emission spectra of complexes **1-6** in CH_3CN. The emission lifetimes and quantum yields in CH_3CN are listed in Table 1. The emission spectra, lifetimes, and quantum yields in other solvents are provided in ESI Fig. S3 and Table S4. The emission energies and spectral features of complexes **1-3** resemble each other, with emission maxima near 590 nm and a shoulder around 615 nm. The lifetimes in deoxygenated solutions of **1-3** are similar (~2.5-3.0 μs in all solvents studied except that the lifetime of **2** in CH_3CN (400 ns) is much shorter). These features indicate that the origin of the emitting states for these complexes should be the same, *i.e.* likely the ^{3}MLCT/^{3}LLCT states with the electrons presumably localized on the phenyl ring of the cyclometalating ligand and the *d*-orbital of the Ir(III), and holes on the dpq (dipyrido[3,2-d:2',3'-f]quinoxaline) part of the diimine ligand. A lack of correlation between the emission energy and π-conjugation of the diimine ligand as well as emission assigned to the ^{3}MLCT/^{3}LLCT state have been reported for Ru(II) complexes with dppz and dppn ligands.[21]

For complexes **4-6**, the emission features (such as energies, lifetimes and shapes) are drastically different. When the π-conjugation of the cyclometalating ligand increased from complex **4** to **5**, the emission energy significantly decreased (λ_{em} changed from 554 nm for **4** to 629 nm for **5**). However, the emission lifetimes of **4** and **5** were on the same order of magnitude in all solvents studied. In view of their structureless emission spectra, the thermally induced Stokes shifts (see ESI Fig. S4), and their lifetimes, we tentatively assign the emission from these two complexes to ^{3}MLCT/^{3}LLCT states with the electrons presumably localized on the coordinating phenyl ring of the cyclometalating dpp or dpqx ligand and the *d*-orbital of the Ir(III), and holes on the dppn ligand. The red-shifted emission of **5** could probably be attributed to the better electron delocalization on the dppn ligand in **5** compared to that in **4**, which stabilized the dppn based holes in **5**. Although the NTOs corresponding to the triplet transitions contributing to the emitting states of **1-6** were unavailable at this time, the ^{1}MLCT/^{1}LLCT transitions in **4** (S_3 state) and **5** (S_1 state) (see the NTOs in Table 2) clearly indicated the more electron density delocalization on the dppn based electrons in **5**. Assuming the NTOs representing the triplet transitions contributing to the emission have the similar characteristics to the NTOs representing the ^{1}MLCT/^{1}LLCT transitions, it is easy to understand the red-shifted emission of **5** with respect to that of **4**.

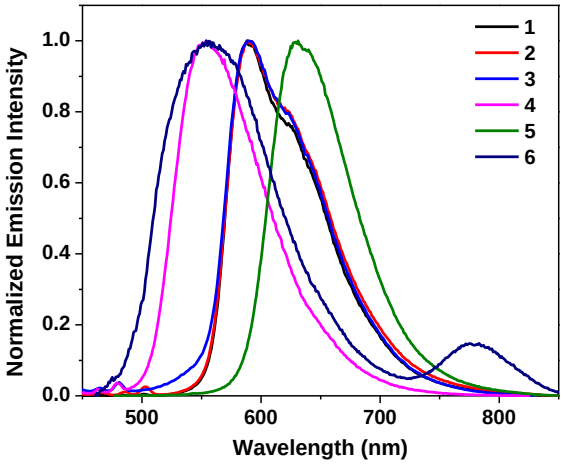

Fig. 3 Normalized emission spectra of complexes **1-6** in deoxygenated acetonitrile. The excitation wavelength was 435 nm for **1**, 436 nm for **2**, 419 nm for **3**, 418 nm for **4**, 466 nm for **5**, and 436 nm for **6**. The concentration used was 1×10^{-5} mol/L.

The emission of **6** is distinct from all of the other complexes. This complex exhibited dual emission, with a broad high-energy emission band at 553 nm and a low-energy emission band at 774 nm. The excitation spectra monitored at the band maxima of these two emission bands were different (see ESI Fig. S5), indicating the different natures of the emitting states. Considering the similar energy of the high-energy emission band of **6** to that of **4**, we attribute this emission originating from the ^{3}MLCT/^{3}LLCT states. For the low-energy emission band at 774 nm, we ascribe it predominantly to the dpbq localized ^{3}ILCT/$^3\pi,\pi^*$ emission. Such an assignment is primarily based on the similar energy of this band to the phosphorescence energy of the dpbq ligand (765 nm, see ESI Fig. S6). The possibility of this low-energy emission band arising from the trace amount of dpbq ligand or the $[(dpbq)_2IrCl]_2$ dimer precusor has been excluded based on the following facts: First, TLC analysis and elemental analysis results confirmed the ≥99.5% purity of complex **6**; secondly, the emission spectra obtained at a varity of excitation wavelengths all had the same dual emission feature, indicating the dual emission arising from a single species; thirdly, if trace amount of dpbq ligand was present in the complex, its fluorescence at 480 nm should be observed upon excitation at the UV region, however, it was not detected; fourthly, even if trace amount of $[(dpbq)_2IrCl]_2$ was present, its emission at 780 nm was extremely weak, which could not give the detectable signals at 774

View Article Online DOI: 10.1039/C6DT02416F

nm. Therefore, we believe the dual emission truly emanating from complex **6**. It should be pointed out that although dual emission is an uncommon feature, it has been well documented in the literture for transition-metal complexes including Ir(III) and Ru(II) complexes.[20a,30] The distinct nature of the emitting states for complexes **4-6** clearly reflects the impact of the extended π-conjugation of the cyclometalating ligand on the emission, which shifted the emitting state from ^{3}MLCT/^{3}LLCT in **4** and **5** to the dpbq ligand-based ^{3}ILCT state in **6**. This effect was quite different from that observed with extending π-conjugation on the diimine ligand, which essentially shows no impact on the emission energy of the Ir(III) complexes.

Transient difference absorption

In order to further understand how the extended π-conjugation on the diimine and/or cyclometalating ligand influences the triplet excited-state characteristics, nanosecond transient absorption (TA) experiments were carried out to investigate the triplet excited-state absorption and lifetime, as well as the triplet quantum yield. The TA spectra of complexes **1-6** in deoxygenated acetonitrile at zero delay after 355 nm excitation are illustrated in Fig. 4, and the time-resolved spectra for each complex are provided in ESI Fig. S8.

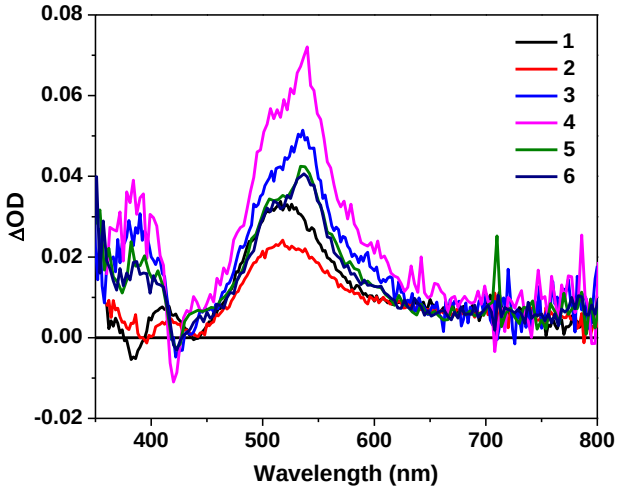

Fig. 4 Nanosecond transient absorption spectra of complexes **1-6** in deoxygenated acetonitrile at zero delay after 355 nm excitation. A_{355} = 0.4 in a 1-cm cuvette.

The TA spectral features for complexes **1** and **2** were similar, and their TA lifetimes agreed with their emissive lifetimes. These characteristics suggest that the excited state giving rise to the observed TA is also the emitting ^{3}MLCT/^{3}LLCT state. In contrast, the TA spectra of **3-6** are similar to each other, but different from those of **1** and **2**. The TA lifetimes measured for **3-6** were much longer than their respective emission lifetimes. In addition, the TA spectral features of complexes **3-6** all resemble those of the dppn ligand (see ESI Fig. S7) and the Ru(II) complex bearing the dppn ligand.[21] Thus, the triplet excited state giving rise to the observed TA spectra for these four complexes should predominantly be the dppn ligand-localized $^3\pi,\pi^*$ state. However, in view of the shorter lifetimes of **6** in comparison to those of **3-5**, the ^{3}ILCT states may contribute to the transient signal of **6** as well. The presence of a non-emissive low-energy, long-lived $^3\pi,\pi^*$ state and an emissive short-lived CT excited state has been previously reported for some Ru(II)[21,31] and Pt(II) complexes.[32] This phenomenon suggests that the ^{3}CT state and $^3\pi,\pi^*$ state are not thermally equilibrated. Moreover, we speculate that the decay from the high-lying ^{3}CT state via nonradiative process to the low-lying $^3\pi,\pi^*$ state is very inefficient or completely blocked for reasons that are not well understood, which makes the emission from the high-lying ^{3}CT state possible.

It is worth noting that although the nature of the emitting state for complexes **3-6** varies, their lowest triplet excited states remain centered on the extended π-expansive dppn ligand. With the increased π-conjugation on the C^N ligand, the dpbq-based ^{3}ILCT state could mix with the dppn $^3\pi,\pi^*$ state due to a decreased energy of the ^{3}ILCT state that lies in proximity to the dppn $^3\pi,\pi^*$ state.

Reverse saturable absorption (RSA)

It is well known that RSA occurs when excited-state absorption is stronger than ground state absorption. The TA spectra of complexes **1-6** clearly demonstrates a strong positive absorption band in the region of 450-800 nm, suggesting stronger excited-state absorption compared to the ground-state absorption. Therefore, it is reasonable to expect a strong RSA in this spectral region. Nonlinear transmission experiments were carried out to manifest the RSA at 532 nm using a 4.1-ns pulsed laser. The transmittance vs. incident energy curves for complexes **1-6** are presented in Fig. 5.

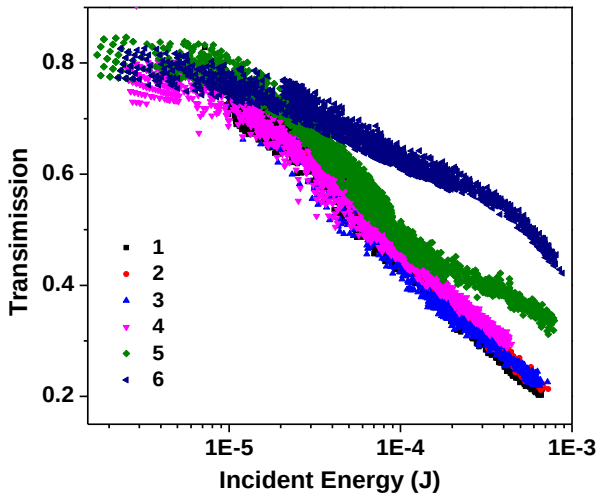

Fig. 5 Transmittance vs. incident energy curves of complexes **1-6** in acetonitrile in a 2-mm cuvette for 4.1 ns laser pulses at 532 nm. The linear transmission of the sample solutions were adjusted to 80% at 532 nm in the 2-mm cuvette. The radius of the beam waist at the focal plane was approximately 96 μm.

All complexes exhibited a moderate to strong transmission decrease with increasing incident energy, a clear indication of RSA. The degree of RSA for complexes **1-4** was similar, and was comparable to the benchmark Ir(III) complexes with π-conjugated

View Article Online DOI: 10.1039/C6DT02416D

aromatic substituents appended to diimine or cyclometalating ligands.[7d,20c,23,33] In contrast, RSA decreased in complexes **5** and **6** in comparison to those of **1**-**4**. Our previous studies on RSA materials revealed that the key parameter in determining the degree of RSA is the ratio of the excited-state absorption cross section to the ground-state absorption cross section (σ_{ex}/σ_0). The σ_0 can be deduced from the molar extinction coefficient at 532 nm from the UV-vis absorption data, while the σ_{ex} can be estimated from the ΔOD values at the TA band maximum and 532 nm, and the $\varepsilon_{T1\text{-}Tn}$ value at the TA band maximum wavelength using the method described previously by our group.[34] The values obtained are presented in Table 3. Due to very efficient heavy-atom induced ISC in the Ir(III) complexes, the RSA of ns laser pulses could mainly arise from the triplet excited-state absorption rather than the singlet excited-state absorption. Thus the quantum yield of the triplet excited state should play a significant role in determining the degree of RSA. Considering these factors, the $\sigma_{ex}\Phi_T/\sigma_0$ ratios for complexes **1**-**6** roughly correlate to the observed RSA trend for these complexes. With the increased π-conjugation on the cyclometalating ligand, the ground-state absorption at 532 nm drastically increased in **5** and **6**, which reduced the σ_{ex}/σ_0 ratio and thus decreased the RSA at 532 nm. However, the broadened ground-state absorption into the near-IR region would broaden the RSA region for complex **6**, making it a potential broadband RSA complex.

Table 3 Ground-state and excited-state absorption cross sections of complexes **1**-**6** in acetonitrile.

	1	**2**	**3**	**4**	**5**	**6**
σ_0 / 10^{-18} cm^2	1.6	1.6	3.9	2.5	8.4	15.7
σ_{ex} / 10^{-18} cm^2	270	710	780	380	730	130
σ_{ex}/σ_0	173	432	197	151	87	8
$\sigma_{ex}\Phi_T/\sigma_0$	43	22	24	35	6	0.4

Photodynamic therapy (PDT)

Reports on the use of Ir(III) complexes as PSs for PDT are rare.[35] Due to the exceptionally long-lived triplet excited states of complexes **3**-**6** measured by TA (as long as ~40 μs), it was reasonable to propose that these complexes could be good candidates for PDT applications. We have previously shown that Ru(II)-based metal-organic dyads possessing long-lived triplets contributed by π-expansive organic units with low-energy excited states (≤ 2.1 eV) have proven to be highly effective as PDT agents.[22,25,36] The requirement appears to be a $^3\pi,\pi^*$ state that is in close energetic proximity to the ^{3}MLCT state, which lies at approximately 2.1 eV for typical Ru(II) polypyridyl complexes. We hypothesize that slow ISC from triplet excited states with substantial organic character provides ample opportunity for bimolecular reactions with oxygen and other quenchers.

To demonstrate that this concept could be operative in Ir(III) systems, the photobiological activities of **1**-**6** were assessed in terms of dark and light EC_{50} values and phototherapeutic indices (PIs) using two cancer cell lines and two irradiation conditions (Table 4). Briefly, EC_{50} refers to the effective concentration required to reduce cell viability by 50%, and PI is the ratio of dark to light EC_{50} values. Light treatments consisted of broadband visible or red light irradiation (100 J/cm^2) delivered 16 h after cells were dosed with a given complex. In comparison to the relatively few PI values reported for the other Ir(III) complexes,[35f,35h] complexes **1**-**6** yielded the most potent photocytotoxicities and largest PIs reported to date towards SK-MEL-28 and HL60 cell lines upon broad visible or red light activation. It should be noted that previous reports of photoactivatable Ir(III) complexes utilized UV or blue (425 nm) light. Such high photon energy excitation would be expected to yield even greater photobiological activity from the present series, but these wavelengths are of less interest for practical application.

In general the Ir(III) complexes investigated were more potent toward SK-MEL-28 melanoma cells than HL60 leukemia cells regardless of whether a light trigger was applied, except for complex **6** which was more cytotoxic toward HL60 cells in the dark. Notably, **6** also produced the largest PI of the series in both cell lines (SK-MEL-28, PI>400; HL60, PI>140) with submicromolar visible light EC_{50} values (350-600 nM). The PDT effect observed for **6** was attenuated approximately 10-fold with red light activation but was still more than 40% larger than the best reported to date with *UV light activation* towards HeLa cells[35f] (Fig. 6). Had the previous reports used low-energy red light, this difference would have been much larger. The large PDT effects of **6** upon both visible and red light irradiation could partially be attributed to the broader and stronger absorption in the visible and red regions in comparison to the other complexes investigated in this work, which would populate more PSs to the excited states under identical light fluence and thus enhance the PDT effects. However, we demonstrated the feasibility of utilizing the blue-green absorbing $[Ru(bpy)_2dppn]^{2+}$ complex for effective red or NIR PDT even if the number of absorbed photons was extremely low ($\varepsilon << 100$ M^{-1}cm^{-1}) in the red-NIR region.[25] The efficient PDT at low photo absorption was attributed to the extremely photosensitizing long-lived $^3\pi,\pi^*$ configuration. Taking into account of this finding and the lack of correlation between the light absorptivity and PIs for complexes **1**-**5**, we speculate that the strong PDT effect of **6** could be mainly ascribed to the extremely high photosensitization efficiency of the $^3\pi,\pi^*$ configuration although the strong and broad absorption in the visible to the NIR region also contribute.

Table 4 (Photo)cytotoxicity of complexes **1**-**6** towards SK-MEL-28 and HL60 cells.

		Dark	Vis PDT		Red PDT	
		EC_{50} (μM)	EC_{50} (μM)	PI	EC_{50} (μM)	PI
SK-MEL-28	**1**	0.40±0.07	0.004±0.001	100	0.19±0.01	2.1
	2	0.27±0.04	0.003±0.001	90	0.034±0.002	7.9
	3	1.53±0.03	0.019±0.002	81	0.25±0.03	6.1
	4	2.11±0.13	0.029±0.003	72	1.83±0.08	1.2
	5	1.37±0.07	0.062±0.008	22	0.65±0.07	2.1
	6	144±56.9	0.354±0.066	407	4.45±0.08	32
HL60	**1**	0.43±0.03	0.017±0.001	25	0.16±0.01	2.7
	2	0.41±0.04	0.010±0.001	41	0.11±0.02	3.7
	3	1.57±0.05	0.06±0.01	26	0.54±0.02	2.9
	4	4.51±0.13	0.049±0.002	92	2.41±0.08	1.9
	5	1.39±0.31	0.117±0.006	12	0.90±0.03	1.5
	6	83.9±1.40	0.588±0.052	143	5.33±0.37	16

Of considerable importance for PDT applications in particular, complex **6** was the only PS in the series that could be considered

nontoxic without a light trigger (dark EC_{50} >100 μM), which was the source of the large phototherapeutic margin. To the best of our knowledge, all other phototoxic Ir(III) complexes reported to date have considerable dark cytotoxicity. Typically these EC_{50} values are between 30 and 50 μM,[35f] with some being as low as 8 μM.[35g] Similar observations have been made for cyclometalated Ru(II) complexes.[37] Complexes **1** and **2** produced submicromolar toxicity in the absence of any light trigger (Table 4 and ESI Fig. S9), and complexes **3**-**5** displayed dark toxicity with EC_{50} values ranging from 1 to 5 μM. Despite PIs of up to 100, complexes **1**-**5** may be better suited as traditional anticancer agents provided there is some selectivity toward cancer cells over normal cells. For example, complex **2** is 100-fold more potent than cisplatin toward melanoma cells, and efforts are underway to probe for selectivity.

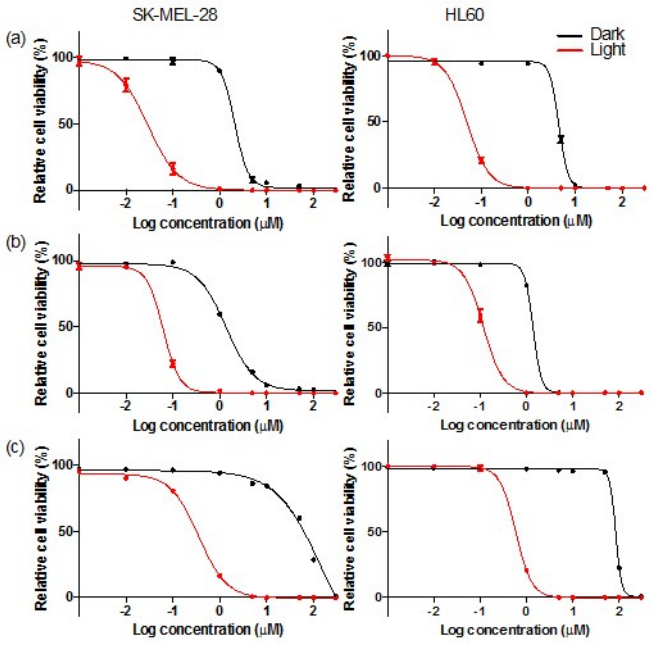

Fig. 6 In vitro dose-response curves for complexes **4** (a), **5** (b) and **6** (c) in SK-MEL-28 cells (left column) and HL60 cells (right column) with visible light activation.

The emission observed from **1**-**6** could be used to track cellular accumulation and distribution due to relatively bright intracellular luminescence (Figs. 7-8 and ESI Figs. S10-S11). Laser scanning confocal microscopy was used to detect the complexes in SK-MEL-28 melanoma cells after a short incubation period (15 min). Cellular uptake occurred both with and without a light trigger for all of the complexes. However, the application of a light trigger influenced the distribution of the PSs within the cell. For example, localization in the membrane was evident for complexes **1**-**3** prior to light treatment (ESI Fig. S10). Application of a sublethal visible light treatment of 50 J/cm^2 caused the PSs to move from the cell membrane to the cytosol and mitochondria. Complexes **4**-**6** accumulated throughout the cell without light activation, with some preference for the nuclei of adherent cells and the cytosol of the suspension phenotype. Upon light activation, complexes **4** and **5** caused a significant change in cell shape such that it was difficult to compare localization trends, but **6** was relocalized from nuclei to cytoplasm. While these changes are not conclusive of a particular type of cell death, they do serve to highlight the utility of such complexes as *theranostic* agents, namely they integrate diagnostic capability with therapeutic capacity. Such platforms are of great interest in photomedicine.

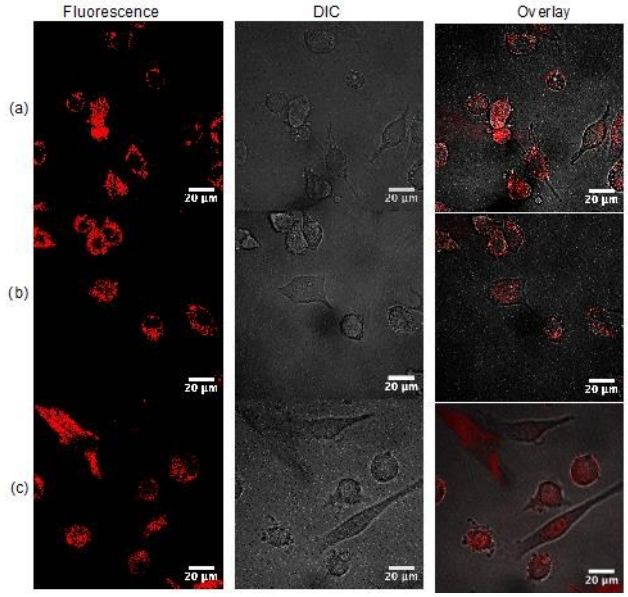

Fig. 7 Confocal luminescence images of SK-MEL-28 cells treated with 50 μM complex **4** (a) or **5** (b) and **6** (c) in the dark.

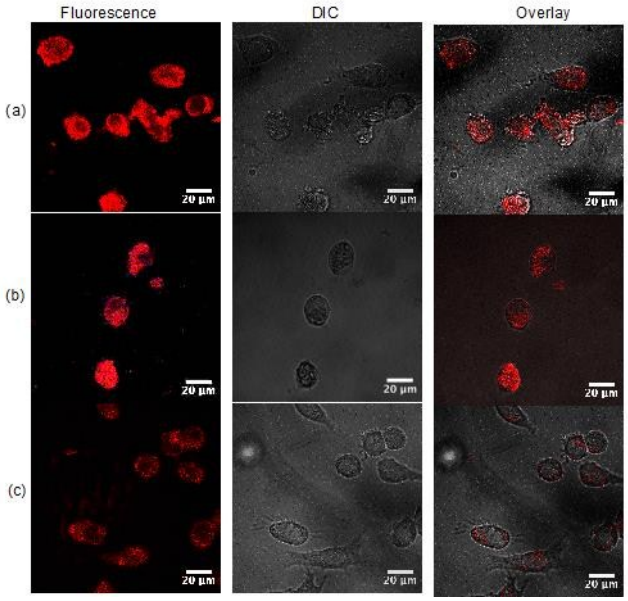

Fig. 8 Confocal luminescence images of SK-MEL-28 cells treated with 50 μM complex **4** (a) or **5** (b) and **6** (c) with a visible light treatment (50 J/cm^2).

Because some of the PSs appeared to accumulate in the nuclei of cells, complexes **1**-**6** were probed for their abilities to interact with plasmid DNA with and without a light treatment. Topological

View Article Online
DOI: 10.1039/C6DT02155F

changes to plasmid DNA exposed to various exogenous agents and treatment conditions can be readily discerned by changes in electrophoretic mobility of the DNA through an agarose gel slab. Under the gel electrophoresis conditions employed (Fig. 9 and ESI Fig. S12), the relative migration distances of plasmid DNA increase in the order of aggregated (Form IV, induced aggregation or condensation), nicked circular (Form II, single-strand breaks), linear (Form III, two single-strand breaks in close proximity on opposite strands or frank double-strand breaks), and supercoiled (Form I, no strand scission).

Plasmid pUC19 DNA (20 μM nucleotide phosphates) was dosed with complexes **1**-**6** at concentrations between 5 and 100 μM (PS-to-nucleotide ratios 0.25-5). The samples were either kept in the dark or irradiated with visible light (14 J/cm^2) and then electrophoresed on 1% agarose gels in 1× TAE for 30 min. The irradiation conditions used for the DNA experiments were intentionally "softer" than those used for the cellular assays to ensure that light did not damage the DNA in the absence of PS. Complexes **1**-**3** caused aggregation of plasmid DNA in a concentration-dependent manner regardless of whether a light treatment was applied (ESI Fig. S12, lanes 8-9). The major difference between the dark and light treated samples was that photoactivation of complexes **1**-**3** produced a slight increase in Form II DNA concomitant with a decrease in Form I with increasing concentration of PS in the order of **3** > **2** > **1**. As expected, the extent of PS-induced aggregation also followed this order and was in agreement with what has been observed with increasing π-expansion, and thus intercalating power, on diimine ligands in certain Ru(II) complexes. Complexes **1**-**3** did not appear to interefere with the ability of ethidium bromide (EtBr) to intercalate and stain the DNA.

When π-conjugation was increased on the cyclometalating ligand, PS-induced DNA aggregation also increased in the order of **6** > **5** > **4**, with complexes **4** and **5** showing very little Form IV DNA on the gel with or without a light trigger (Fig. 9). As observed for **1**-**3**, a slight increase in Form II over Form I occurred but was barely detectable by eye. Unlike complexes **1**-**3**, **6** showed a marked difference in PS-induced DNA aggregation between the dark and light-treated samples. Light activation of **6** produced 100% Form IV DNA, while the dark treatment produced very little aggregated DNA with no change in the relative amounts of Forms I and II. Complex **5** behaved differently than the rest of the photoactivated complexes in that it caused the DNA bands on the gel to disappear at higher concentrations with no influence on the dark sample. Quenching of EtBr luminescence, competition for EtBr binding sites, or distortion of the helix to prevent EtBr binding are normally implicated in the lack of DNA staining by treated samples, especially at higher concentrations of the exogenous agent. However, the dark sample treated with **5** at high concentration did show luminescence from intercalated EtBr. Therefore, light activation of **5** must influence its binding mode and/or interaction with EtBr in a substantial way.

It is interesting to note that the Ir(III) complex yielding the largest PI of the series with no dark toxicity toward cells (*i.e.* complex **6**) was the only one that showed a clear difference in PS-induced aggregation of DNA between dark and light-treated samples. While DNA may not be the intracellular target, these results do suggest that there is a noticeable difference in the way complex **6** interacts with a biological target such as DNA when activated by light. Such a difference could also be applicable for interactions with potential non-genomic targets as well as cellular uptake, efflux, metabolism, and localization. Typically singlet oxygen generators that bind DNA well produce notable conversion of Form I DNA to Form II in this gel mobility shift assay. The lack of significant Form II production coupled with clear evidence of DNA interactions via aggregation points toward the involvement of other reactive intermediates for cellular damage (unless DNA interactions suppress this sensitization pathway for some reason).

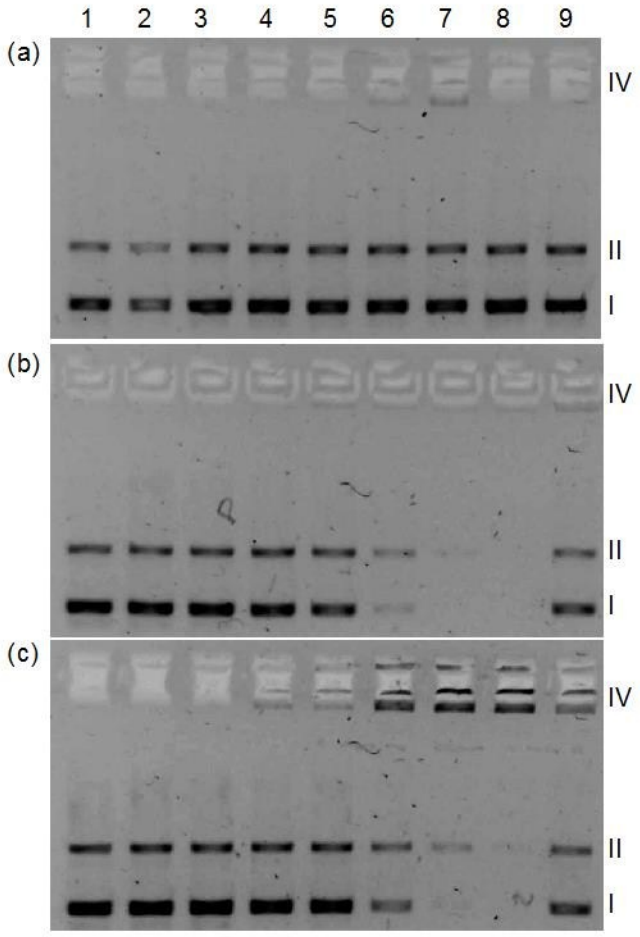

Fig. 9 DNA photocleavage of pUC19 DNA (20 μM bases) dosed with metal complex (MC) **4** (a), **5** (b) or **6** (c) and visible light (14 J/cm^2). Gel mobility shift assays employed 1% agarose gels (0.75 μg/mL ethidium bromide) electrophoresed in 1× TAE at 8 V/cm for 30 min. Lane 1, DNA only (*-hv*); lane 2, DNA only (*+hv*); lane 3, 5 μM MC (*+hv*); lane 4, 20 μM MC (*+hv*); lane 5, 40 μM MC (*+hv*); lane 6, 60 μM MC (*+hv*); lane 7, 80 μM MC (*+hv*); lane 8, 100 μM MC (*+hv*); lane 9, 100 μM MC (*-hv*). Forms I, II, and IV DNA refer to supercoiled plasmid, nicked circular plasmid, and aggregated plasmid, respectively.

Experimental section

The details of experiments are described in ESI.†

Conclusions

Six Ir(III) complexes with cyclometalating and diimine ligands bearing different degrees of π-conjugation were synthesized, and their photophysical and photobiological properties were systematically investigated. The natures of the optical transitions were confirmed by TDDFT calculations. Extending the π-conjugation on the diimine ligand mainly influenced ground-state absorption, while the nature of the emitting triplet excited state was not affected. In contrast, extending the π-conjugation on the cyclometalating ligand affects both ground-state absorption and the nature of the emitting triplet excited states. However, the lowest-energy triplet excited state for complexes **4-6** did not change. This dppn ligand-localized $^3\pi,\pi^*$ state gave rise to the long-lived, strong excited-state absorption in the visible to the near-IR region. Complexes **1-4** exhibit strong RSA at 532 nm for ns laser pulses which is comparable to the benchmark Ir(III) complex reverse saturable absorbers at 532 nm, while complex **6** shows the potential as broadband reverse saturable absorber at 500-850 nm. Presumbly due to the long-lived $^3\pi,\pi^*$ state and the weak but broad ground-state absorption in the near-IR region, complexes **4-6** elicited photodynamic effects toward cancer cells with low-energy visible and red light. The phototherapeutic margin for complex **6** is the largest for an Ir(III) complex PSs reported to date upon broad visible or red light activation, and its interaction with plasmid DNA suggests that a photocytotoxicity mechanism other than singlet oxygen sensitization may be operative. The Ir(III) complexes also show potential as theranostic agents due to their strong intracellular luminescence.

Acknowledgements

W. Sun acknowledges the financial support from the Army Research Laboratory (W911NF-10-2-0055) for the synthesis and photophysical studies of the complexes reported in this paper. The computational part of the work was supported by NSF (DMR-1411086 and CNS-1229316) to W. Sun and S. Kilina. S.A.M and H.Y. acknowledge financial support from the Natural Sciences and Engineering Council of Canada (NSERC), the Canadian Institutes of Health Research (CIHR), the Canadian Foundation for Innovation (CFI), the Nova Scotia Research and Innovation Trust (NSRIT), and Acadia University.

Notes and references

1 M. Vijayakumar and M. S. Gopinathan, *J. Mol. Struc.: THEOCHEM*, 1996, **361**, 15-19.

2 (a) T. Sajoto, P. I. Djurovich, A. Tamayo, M. Yousufuddin, R. Bau, M. E. Thompson, R. J. Holmes and S. R. Forrest, *Inorg. Chem.*, 2005, **44**, 7992-8003; (b) C. H. Yang, S. W. Li, Y. Chi, Y. M. Cheng, Y. S. Yeh, P. T. Chou, G. H. Lee, C. H. Wang and C. F. Shu, *Inorg. Chem.*, 2005, **44**, 7770-7780; (c) Y. Kawamura, K. Goushi, J. Brooks, J. J. Brown, H. Sasabe and C. Adachi, *Appl. Phys. Lett.*, 2005, **86**, 071104-1 – 071104-3.

3 (a) Z.-Q. Chen, Z.-Q. Bian and C.-H. Huang, *Adv. Mater.*, 2010, **22**, 1534-1539; (b) S. Lamansky, P. Djurovich, D. Murphy, F. Abdel-Razzaq, H. E. Lee, C. Adachi, P. E. Burrows, S. R. Forrest and M. E. Thompson, *J. Am. Chem. Soc.*, 2001, **123**, 4304-4312; (c) C. Adachi, M. A. Baldo, M. E. Thompson and S. R. Forrest, *J. Appl. Phys.*, 2001, **90**, 5048-5051.

4 (a) R. D. Costa, E. Orti, H. J. Bolink, F. Monti, G. Accorsi and N. Armaroli, *Angew. Chem. Int. Ed.*, 2012, **51**, 8178-8211; (b) C.-H. Yang, J. Beltran, V. Lemaur, J. Cornil, D. Hartmann, W. Sarfert, R. Froehlich, C. Bizzarri and L. De Cola, *Inorg. Chem.*, 2010, **49**, 9891-9901.

5 (a) C. Li, J. Lin, Y. Guo and S. Zhang, *Chem. Commun.*, 2011, **47**, 4442-4444; (b) J. Jiang, C. Zhang, W. Lin, Y. Liu, S. Liu, Y. Xu, Q. Zhao and W. Huang, *Macromol. Rapid Commun.*, 2015, **36**, 640-646.

6 (a) Q. Zhao, F. Li and C. Huang, *Chem. Soc. Rev.*, 2010, **39**, 3007-3030; (b) N. Zhao, Y.-H. Wu, L.-X. Shi, Q.-P. Lin and Z.-N. Chen, *Dalton Trans.*, 2010, **39**, 8288-8295.

7 (a) T. M. Pritchett, M. J. Ferry, W. M. Shensky, A. G. Mott, D. J. Stewart, S. L. Long, J. E. Haley, Z. Li and W. Sun, *Opt. Lett.*, 2015, **40**, 186-189; (b) C. Pei, P. Cui, C. McCleese, S. Kilina, C. Burda and W. Sun, *Dalton Trans.*, 2015, **44**, 2176-2190; (c) K.-Y. Kim, R. T. Farley and K. S. Schanze, *J. Phys. Chem. B*, 2006, **110**, 17302-17304;.(d) Y. Li, N. Dandu, R. Liu, L. Hu, S. Kilina and W. Sun, *ACS Appl. Mater. Interfaces*, 2013, **5**, 6556-6570.

8 (a) S. Hirata, K. Totani, T. Yamashita, C. Adachi and M. Vacha, *Nat. Mater.*, 2014, **13**, 938-946; (b) W. Blau, H. Byrne, W. M. Dennis and J. M. Kelly, *Opt. Commun.*, 1985, **56**, 25-29.

9 M. Bass, P. Franken, J. Ward and G. Weinreich, *Phys. Rev. Lett.*, 1962, **9**, 446.

10 W. G. Spitzer, F. Trumbore and R. Logan, *J. Appl. Phys.*, 1961, **32**, 1822-1830.

11 C. Li, L. Zhang, R. Wang, Y. Song and Y. Wang, *J. Opt. Soc. Am. B*, 1994, **11**, 1356-1360.

12 D. J. Harter, M. L. Shand and Y. B. Band, *J. Appl. Phys.*, 1984, **56**, 865-868.

13 G.-J. Zhou and W.-Y. Wong, *Chem. Soc. Rev.*, 2011, **40**, 2541-2566.

14 (a) B. Zhang, Y. Li, R. Liu, T. M. Pritchett, J. E. Haley and W. Sun, *ACS Appl. Mater. Interfaces*, 2013, **5**, 565-572; (b) Y. Fan and D. Zhao, *ACS Appl. Mater. Interfaces*, 2015, **7**, 6162-6171; (c) W. Sun, Z.-X. Wu, Q.-Z. Yang, L.-Z. Wu and C.-H. Tung, *Appl. Phys. Lett.*, 2003, **82**, 850-852; (d) F. Guo, W. Sun, Y. Liu and K. Schanze, *Inorg. Chem.*, 2005, **44**, 4055-4065; (e) W. Sun, B. Zhang, Y. Li, T. M. Pritchett, Z. Li and J. E. Haley, *Chem. Mater.*, 2010, **22**, 6384-6392; (f) P. Shao, Y. Li and W. Sun, *J. Phys. Chem. A*, 2008, **112**, 1172-1179; (g) G.-J. Zhou, W.-Y. Wong, D. Cui and C. Ye, *Chem. Mater.*, 2005, **17**, 5209-5217; (h) G. Zhou, W.-Y. Wong, S.-Y. Poon, C. Ye and Z. Lin, *Adv. Funct. Mater.*, 2009, **19**, 531-544; (i) T. J. McKay, J. Staromlynska, J. R. Davy and J. A. Bolger, *J. Opt. Soc. Am. B*, 2001, **18**, 358-362; (j) T. J. McKay, J. A. Bolger, J. Staromlynska and J. R. Davy, *J. Phys. Chem.*, 1998, **108**, 5537-5541.

15 G. R. Allan, D. R. Labergerie, S. J. Rychnovsky, T. F. Boggess, A. L. Smirl and L. Tutt, *J. Phys. Chem.*, 1992, **96**, 6313-6317.

16 (a) K. B. Manjunatha, R. Dileep, G. Umesh, M. N. Satyanarayan and B. R. Bhat, *Opt. Mater.*, 2014, **36**, 1054-

1059; (b) K. B. Manjunatha, R. Dileep, G. Umesh and B. R. Bhat, *Opt. Laser. Technol.*, 2013, **52**, 103-108.

17 (a) G.-J. Zhou, W.-Y. Wong, C. Ye and Z. Lin, *Adv. Funct. Mater.*, 2007, **17**, 963-975; (b) G.-J. Zhou, W.-Y. Wong, Z. Lin and C. Ye, *Angew Chem. Int. Ed.*, 2006, **45**, 6189-6193.

18 T. J. Dougherty, C. J. Gomer, B. W. Henderson, G. Jori, D. Kessel, M. Korbelik, J. Moan and Q. Peng, *J. Natl. Cancer Inst.*, 1998, **90**, 889-905.

19 B. W. Henderson and T. J. Dougherty, *Photochem. Photobiol.*, 1992, **55**, 145-157.

20 (a) S.-H. Wu, J.-W. Ling, S.-H. Lai, M.-J. Huang, C. H. Cheng and I.-C. Chen, *J. Phys. Chem. A*, 2010, **114**, 10339-10344; (b) Q. Zhao, S. Liu, M. Shi, C. Wang, M. Yu, L. Li, F. Li, T. Yi and C. Huang, *Inorg. Chem*,. 2006, **45**, 6152-6160; (c) R. Liu, N. Dandu, J. Chen, Y. Li, Z. Li, S. Liu, C. Wang, S. Kilina, B. Kohler and W. Sun, *J. Phys. Chem. C*, 2014, **118**, 23233-23246; (d) H.-Y. Chen, C.-H. Yang, Y. Chi, Y.-M. Cheng, Y.-S. Yeh, P.-T. Chou, H.-Y. Hsieh, C.-S. Liu, S.-M. Peng and G.-H. Lee, *Can. J. Chem.*, 2006, **84**, 309-318.

21 Y. Sun, L. E. Joyce, N. M. Dickson and C. Turro, *Chem. Commun.*, 2010, **46**, 2426-2428.

22 R. Lincoln, L. Kohler, S. Monro, H. Yin, M. Stephenson, R. Zong, A. Chouai, C. Dorsey, R. Hennigar, R. P. Thummel and S. A. McFarland, *J. Am. Chem. Soc.*, 2013, **135** (45), 17161-17175.

23 Y. Li, N. Dandu, R. Liu, Z. Li, S. Kilina and W. Sun, *J. Phys. Chem. C*, 2014, **118** (12), 6372-6384.

24 Q.-X. Zhou, W.-H. Lei, J.-R. Chen, C. Li, Y.-J. Hou, X.-S. Wang and B.-W. Zhang, *Chem. Eur. J.*, 2010, **16**, 3157-3165.

25 H. Yin, M. Stephenson, J. Gibson, E. Sampson, G. Shi, T. Sainuddin, S. Monro and S. A. McFarland, *Inorg. Chem.*, 2014, **53** (9), 4548-4559.

26 (a) Z. Molphy, A. Prisecaru, C. Slator, N. Barron, M. McCann, J. Colleran, D. Chandran, N. Gathergood and A. Kellett, *Inorg. Chem.*, 2014, **53**, 5392-5404; (b) F. Miomandre, S. Stancheva, J.-F. Audibert, A. Brosseau, R. B. Pansu, M. Lepeltier and C. R. Mayer, *J. Phys. Chem. C*, 2013, **117**, 12806-12814.

27 M. B. Nonoyama, *Bull. Chem. Soc. Jpn.*, 1974, **47**, 767-768.

28 (a) J. Sun, W. Wu, H. Guo and J. Zhao, *Eur. J. Inorg. Chem.*, 2011, **21**, 3165-3173; (b) F. Neve and A. Crispini, *Eur. J. Inorg. Chem.*, 2000, 1039-1043.

29 R. L. Martin, *J. Chem. Phys.*, 2003, **118**, 4775-4777.

30 (a) E. C. Glazer, D. Magde and Y. Tor, *J. Am. Chem. Soc.*, 2005, **127**, 4190-4192; (b) E. Sakuda, C. Matsumoto, Y. Ando, A. Ito, K. Mochida, A. Nakagawa and N. Kitamura, *Inorg. Chem.*, 2015, **54**, 3245-3252; (c) K. A. King and R. J. Watts, *J. Am. Chem. Soc.*, 1987, **109**, 1589-1590; (d) A. P. Wilde, K. A. King and R. J. Watts, *J. Phys. Chem.*, 1991, **95**, 629-634; (e) S. Ladouceur, L, Donato, M. Romain, B. P. Mudraboyina, M. B. Johansen, J. A. Wisner and E. Zysman-Colman, *Dalton Trans.*, 2013, **42**, 8838-8847; (f) K. Y. Zhang, H.-W. Liu, M.-C. Tang, A. W.-T. Choi, N. Zhu, X.-G. Wei, K.-C. Lau and K. K.-W. Lo, *Inorg. Chem.*, 2015, **54**, 6582-6593; (g) Y.-S. Yeh, Y.-M. Cheng, P.-T. Chou, G.-H. Lee, C.-H. Yang, Y. Chi, C.-F. Shu and C.-H. Wang, *ChemPhysChem*, 2006, **7**, 2294-2297; (h) R. Lincoln, L. Kohler, S. Monro, H. Yin, M. Stephenson, R. Zong, A. Chouai, C. Dorsey, R. Hennigar, R. P. Thummel and S. A. McFarland, *J. Am. Chem. Soc.*, 2013, **135**, 17161-17175; (i) Z. Li, H. Li, B. J. Gifford, W. D. N. Peiris, S. Kilina and W. Sun, *RSC Advances*, 2016, **6**, 41214-41228.

31 (a) Y. Liu, R. Hammitt, D. A. Lutterman, L. E. Joyce, R. P. Thummel and C. Turro, *Inorg. Chem.*, 2009, **48**, 375-385; (b) S. P. Foxon, M. A. H. Alamiry, M. G. Walker, A. J. H. M. Meijer, I. V. Sazanovich, J. A. Weinstein and J. A. Thomas, *J. Phys. Chem. A*, 2009, **113**, 12754-12762; (c) S. P. Foxon, C. Metcalfe, H. Adams, M. Webb and J. A. Thomas, *Inorg. Chem.*, 2007, **46**, 409-416.

32 (a) R. Liu, Y. Li, Y. Li, H. Zhu and W. Sun, *J. Phys. Chem. A*, 2010, **114** (48), 12639-12645; (b) R. Liu, N. Dandu, Y. Li, S. Kilina and W. Sun, *Dalton Trans*., 2013, **42** (13), 4398-4409.

33 Y. Li, N. Dandu, R. Liu, S. Kilina and W. Sun, *Dalton Trans*., 2014, **43** (4), 1724-1735.

34 Y. Li, R. Liu, E. Badaeva, S. Kilina and W. Sun, *J. Phy. Chem. C*, 2013, **117** (11), 5908-5918.

35 (a) P. Majumdar, X. Yuan, S. Li, B. Le Guennic, J. Ma, C. Zhang, D. Jacqueminde and J. Zhao, *J. Mater. Chem. B*, 2014, **2**, 2838-2854; (b) D. Maggioni, M. Galli, L. D'Alfonso, D. Inverso, M. V. Dozzi, L. Sironi, M. Iannacone, M. Collini, P. Ferruti, E. Ranucci and G. D'Alfonso, *Inorg. Chem*., 2015, **54**, 544−553; (c) S. P.-Y. Li, C. T.-S. Lau, M.-W. Louie, Y.-W. Lam, S. H. Cheng and K. K.-W. Lo, *Biomaterials*, 2013, **34**, 7519-7532; (d) A. Kando, Y. Hisamatsu, H. Ohwada, T. Itoh, S. Moromizato, M. Kohno and S. Aoki, *Inorg. Chem.*, 2015, **54**, 5342-5357; (e) Y. Li, C.-P. Tan, W. Zhang, L. He, L.-N. Ji and Z.-W. Mao, *Biomaterials*, 2015, **39**, 95-104; (f) R.-R. Ye, C.-P. Tan, L. He, M.-H. Chen, L.-N. Ji and Z.-W. Mao, *Chem. Commun*., 2014, **50**, 10945-10948; (g) A. Kastl, A. Wilbuer, A. L. Merkel, L. Feng, P. D. Fazio, M. Ocker and E. Meggers, *Chem. Commun.*, 2012, **48**, 1863-1865; (h) L. He, Y. Li, C.-P. Tan, R.-R. Ye, M.-H. Chen, J.-J. Cao, L.-N. Ji and Z.-W. Mao, *Chem. Sci.*, 2015, **6**, 5409-5418.

36 (a) G. Shi, S. Monro, R. Hennigar, J. Colpitts, J. Fong, K. Kasimova, H. Yin, R. DeCoste, C. Spencer, L. Chamberlain, A. Mandel, L. Lilge and S. A. McFarland, *Coord. Chem. Rev.*, 2015, **282-283**, 127-138; (b) M. Stephenson, C. Reichardt, M. Pinto, M. Wächtler, T. Sainuddin, G. Shi, H. Yin, S. Monro, E. Sampson, B. Dietzek and S. A. McFarland, *J. Phys. Chem. A*, 2014, **118** (45), 10507-10521.

37 (a) T. Sainuddin, J. McCain, M. Pinto, H. Yin, J. Gibson, M. Hetu and S. A. McFarland, *Inorg. Chem.*, 2016, **55** (1), 83-95; (b) H. Huang, P. Zhang, H. Chen, L. Ji and H. Chao, *Chem. Eur. J.*, 2015, **21**, 715-725; (c) B. Peña, A. David, C. Pavani, M. S. Baptista, J.-P. Pellois, C. Turro and K. R. Dunbar, *Organometallics*, 2014, **33**, 1100-1103; (d) B. A. Albani, B. Peña, K. R. Dunbar and C. Turro, *Photochem. Photobiol. Sci.*, 2014, **13**, 272-280.